Journal of Solid State Chemistry 182 (2009) 2656–2663

Contents lists available at ScienceDirect

Journal of Solid State Chemistry

journal homepage: www.elsevier.com/locate/jssc

Crystal structures and high-temperature phase transitions of the new ordered double perovskites Sr_2SmSbO_6 and Sr_2LaSbO_6

A. Faik, E. Iturbe-Zabalo, I. Urcelay, J.M. Igartua *

Fisika Aplikatua II Saila, Zientzia eta Teknologia Fakultatea, Euskal Herriko Unibertsitatea, P.O. Box 644, Bilbao 48080, Spain

ARTICLE INFO

Article history:
Received 20 April 2009
Received in revised form
9 July 2009
Accepted 10 July 2009
Available online 19 July 2009

PACS:
61.10.Nz
61.50.Ks
61.66.Fu
64.70.Kb

Keywords:
Double perovskite
X-ray diffraction
Crystal structure
Phase transitions

ABSTRACT

In the present work we report X-ray powder diffraction measurements of Sr_2SmSbO_6 and Sr_2LaSbO_6, at different temperatures. The crystal structures at room temperature of both compounds are determined; and results showing the existence of high-temperature phase transitions in them are presented. Both compounds have double perovskite structure with 1:1 ordered arrangement of the *B* site cations. At room temperature their symmetries are described with the $P2_1/n$ space group, that correspond to the $(a^+b^-b^-)$ tilt system. The evolution with temperature of the structure of both compounds shows the presence of two phase transitions: a discontinuous one, at 885 and 945 K, for Sr_2SmSbO_6 and Sr_2LaSbO_6, respectively; and a continuous one, at 1170 and 118 K, for Sr_2SmSbO_6 and Sr_2LaSbO_6, respectively, with the following phase transition sequence: $P2_1/n \rightarrow R\bar{3} \rightarrow Fm\bar{3}m$.

1. Introduction

In two recent works, we analyzed the double perovskite oxides Sr_2AlSbO_6 and Sr_2CoSbO_6 [1] by means of X-ray powder diffraction, and we have reinvestigated the structure at room temperature and the phase transitions at high- and low-temperature of Sr_2CrSbO_6 [2], by X-ray and neutron powder diffraction. At room temperature the crystal structure of Sr_2AlSbO_6 is cubic (space group $Fm\bar{3}m$), with $a = 5.6058(1)$ A. Low-temperature Raman spectroscopic measurements demonstrated that the cubic phase of Sr_2AlSbO_6 is stable down to 79 K. The room-temperature crystal structure of Sr_2CoSbO_6 is trigonal (space group $R\bar{3}$) with $a = 5.6058(1)$ A and $c = 13.6758(3)$ A. At 470 K, however, the material undergoes a continuous phase transition and its structure is converted to cubic (space group $Fm\bar{3}m$). The studied Sr_2CoSbO_6 sample was partially ordered, but unlike Sr_2AlSbO_6, no indication of the formation of anti-phase domains was observed. The Rietveld analysis revealed that Sr_2CrSbO_6 crystallizes at room temperature in a monoclinic system having a space group $I2/m$, with $a = 5.5574(1)$ A, $b = 5.5782(1)$ A, $c = 7.8506(2)$ A and $\beta = 90.06(2)^\circ$, and no $P2_1/n$ space group, as was previously reported. The high-temperature study has shown that the compound presents the following temperature induced phase transition sequence: $I2/m \rightarrow I4/m \rightarrow Fm\bar{3}m$. The low-temperature study demonstrated that the room-temperature $I2/m$ monoclinic symmetry seems to be stable down to 100 K.

The aim of the present work is to analyze the room-temperature structures and the possible temperature-induced structural phase transitions of Sr_2SmSbO_6 and Sr_2LaSbO_6, as there are no previous studies neither on room temperature nor on the temperature-dependent structural modifications of these materials. This work is a part of a systematic study that we have undertaken on the $AA'BSbO_6$ ($AA' = Ca_2, SrCa, Sr_2$) and ($B =$ Al, Co, Cr, Fe, Sc, ...) family of materials.

2. Experimental

2.1. Sample preparation

Sr_2SmSbO_6 and Sr_2LaSbO_6 were prepared by conventional solid state reaction from $SrCO_3$ (99.995%), Sb_2O_5 (99.99%) and Sm_2O_3 (99.999%) or La_2O_3 (99.999%) powders mixed in stoichiometric proportions. All compounds were used as received from Sigma-Aldrich. The starting materials were mixed and ground in an agate mortar with acetone and subsequently heated in air, in alumina

* Corresponding author.
E-mail address: josu.igartua@ehu.es (J.M. Igartua).

0022-4596/$ - see front matter © 2009 Elsevier Inc. All rights reserved.
doi:10.1016/j.jssc.2009.07.021

crucibles. The following heat treatment was used: 6 h at 870 K, to eliminate the organic materials; 24 h at different temperatures, from 1070 to 1770 K every 100 K. After each heating, the samples were cooled down slowly (3 K/min); and re-ground (re-mixed) to improve homogeneity. In order to control the quality of the obtained material, X-ray diffraction measurements were performed after each heating. No impurity phases were detected in the final Sr_2LaSbO_6 material, which has a white color; in the Sr_2SmSbO_6 material, though, which is also white in color, a small quantity (2.7% weight fraction) of Sm_2O_3 was found.

2.2. X-ray powder diffraction measurements

High-quality room-temperature diffraction data were obtained on a Bruker D8 Advance diffractometer equipped with a primary germanium parafocusing monochromator and Bragg–Brentano geometry, using Cu$K\alpha1 = 1.5406$ (A) radiation. A Sol-X energy dispersive detector was used, with a detection window optimized for Cu$K\alpha1$, in order to avoid the fluorescence radiation from the samples. The data were collected between 15° and 110° in 2θ, with steps of 0.01° (2θ) and a counting time of 12 s per step.

High temperature diffraction data from Sr_2MSbO_6 (M = Sm, La) were collected on a similar diffractometer, but equipped with a Våntec high speed one-dimensional detector (with 3° of angular aperture), using Cu$K\alpha$ radiation. An Anton Paar HTK2000 high-temperature chamber with direct sample heating (Pt filament) and a temperature stability of 0.5 K was used. The specimens for high temperature measurements were prepared as described in [1]. In order to obtain reliable values for the unit cell parameters at high temperatures, 43 diffraction patterns, covering the 15−120° 2θ interval, were collected between 675 and 1305 K, with a temperature step of 15 K.

The Rietveld refinement of the structures was performed using the WinPlotr/FullProf package [3]. The peak shape was described by a pseudo-Voigt function, and the background level was modeled using a polynomial function. The refined parameters were: background coefficients, scale factor, lattice constants, atomic positions, independent isotropic atomic displacement parameters, zero shift, peak profile and asymmetry parameters. The Sm_2O_3 (2.7%) impurity was introduced in the refinements as an additional known phase, but without refining it.

3. Results and discussion

3.1. Room-temperature structures of Sr_2SmSbO_6 and Sr_2LaSbO_6

The diffraction patterns collected from Sr_2SmSbO_6 and Sr_2LaSbO_6 at room temperature are shown in Fig. 1(a) and (b), respectively. Many diffraction lines are clearly split, indicating that the unit cells of these materials are distorted, with respect to the aristotype cubic phase characteristic of the double perovskites. The profile matching results suggested the monoclinic symmetry. The usual monoclinic space groups encountered in the double perovskite oxides are $P2_1/n$ and $I2/m$, which give rise, apparently, to the same distortion (in Glazer's notation [4], the tilt systems are $(a^+a^-a^-)$ and $(a^0a^-a^-)$, respectively, thus in the former there is a tilt which is not present in the later), but $P2_1/n$ space group, as is associated with a primitive unit cell, gives rise to super-cell reflections, forbidden in the case of $I2/m$. This is a common place in distorted double perovskites. It is shown in [5], that the diffraction pattern for a compound that has $P2_1/n$ symmetry must have reflections indicative of A-cation displacements (*eeo*), in-phase tilting distortions (*ooe*), out-of-phase tilting distortions and cation ordering (*ooo*). As revealed by the careful examination of the peak splitting patterns from our X-ray powder diffraction (XRPD) diffractograms in both compounds, the unit cells are monoclinic, and the presence of reflections with (*ooe*) cubic indices indicates that there is in-phase tilting. Besides, the usually small reflections corresponding to atomic displacements (*eeo*) are clearly observed in both compounds. Thus, the peak splitting pattern and cubic Miller indices indicate that the symmetry of these compounds is $P2_1/n$. As the starting model for the Rietveld refinements we used the structure reported for another member of the antimony family (Sr_2FeSbO_6), which has been reported to have a room-temperature monoclinic symmetry with the $P2_1/n$ space group [6].

In the insets graph of Fig. 1(a) and (b), we have plotted two 2θ intervals: the first one corresponds to the monoclinic primitive peaks $(\bar{1}11)$ and (111), observed about $2\theta \approx 24°$; and the second one, at about $2\theta \approx 80°$, corresponds to the monoclinic splitting of the (444) cubic reflection into the (044), $(\bar{4}04)$ and (404) reflections. The refinements show that the Sm^{3+} (La^{3+}) and Sb^{5+} ions are regularly ordered at the B and B' sites of the double perovskite. The ionic radii of Sm^{3+} and La^{3+} are 0.958 and 1.032, respectively. The big difference between the ionic radii of Sm^{3+} (La^{3+}) and Sb^{5+} ($r = 0.60$ A) has a strong tendency to order B^{3+} and Sb^{5+} in B and B' sites, respectively.

The results of the refinements are also shown in Fig. 1(a) and (b), and the structural details of Sr_2SmSbO_6 and Sr_2LaSbO_6 at room temperature are given in Tables 1 and 2, respectively. A large deviation of the monoclinic β angle from 90° for both structures can be observed. For the double perovskites with $P2_1/n$ symmetry, it has been reported that, in general, the deviations of the monoclinic angle from 90° are sometimes larger in compounds where one of the octahedral cations, such a rare earth cation, has a fairly large radius [7]. This large deviation can be attributed to the high distortions of the octahedra caused by the large cationic radius.

The tolerance factor values t, $t = (r_{Sr} + r_O)/\sqrt{2}(\bar{r}_{B,Sb} + r_O)$ where $\bar{r}_{B,Sb}$ is the averaged ionic radii of the B and the Sb cations in the double perovskite, for Sr_2SmSbO_6 and Sr_2LaSbO_6 are 0.922 and 0.906, respectively (calculated using the ionic radii suggested in [8]). Increasing the cation size of the central cation in one of the octahedra, gives rise to a more distorted structure: this behavior has also been observed in the tungsten family. In this case, the difference between the sizes of the cations, Sm^{3+} and La^{3+}, is not too big: $\Delta r_{La-Sm} = 0.074$ A; although it is bigger than the difference, for instance, between the Ca^{2+} and the Cd^{2+} cations' radii: $\Delta r_{Ca-Cd} = 0.05$ A, in the tungsten family, in which different grade of distortions were also observed. On the other hand, if we take into account the t values of some other members of the antimony family (Table 1 in [1]), both compounds match perfectly in the table. Both values of t are lower than $t = 0.931$ calculated for Sr_2DySbO_6, which has the lowest t value in the table, with the lowest symmetry $P2_1/n$, which is the one we have obtained for the title compounds.

The mean interatomic distances and some selected bond angles for Sr_2SmSbO_6 and Sr_2LaSbO_6 are listed in Table 3. For the Sb–O bonds, the average values of the bond distances within the octahedra are 1.998 and 2.007, for Sr_2SmSbO_6 and Sr_2LaSbO_6, respectively. For the B–O bonds, the average values are 2.332 for the samarium compound and 2.417 for the lanthanum compound. As mentioned, there is a large size difference between the two B-type cations, the Sb^{5+} cation is much smaller than the Sm and the La cations. In both compounds, the Sm and the La cations are over-bonded, 3.09 for both cations Sm and La, with the Sm–O (La–O) bond lengths being (a little bit) shorter than the expected values obtained by calculating the distances in the bond-valence method [9]. On the other hand, the mean B–O bond lengths of Sb, Sm and La are the expected value from ionic radii giving bond-valence

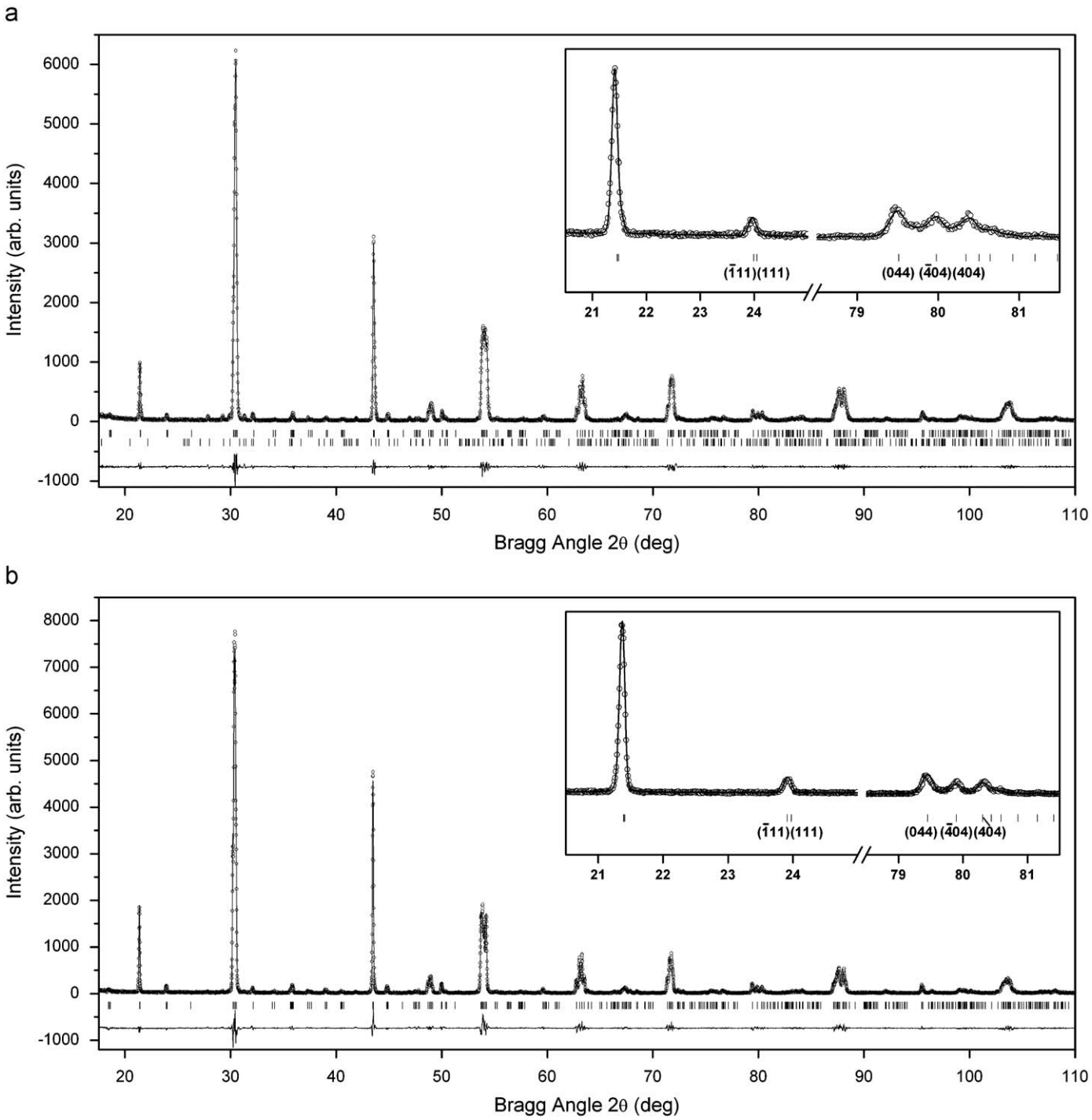

Fig. 1. Experimental (symbols) and calculated (line) powder diffraction profiles for the Rietveld refinement of (a) Sr_2SmSbO_6 and (b) Sr_2LaSbO_6 at room temperature, using a structural model with $P2_1/n$ space group. The bars in the lower part of the graphics represent the Bragg peak positions. In (a), the upper set of bars correspond to the main phase Sr_2SmSbO_6, and the lower set of bars correspond to the impurity Sm_2O_3 (2.7%).

sums in agreement with the formal valence of Sb^{5+}, Sm^{3+} and La^{3+} cations.

The Sr^{2+} cations are located in the cavities formed by the corner-sharing octahedra. The analysis of Sr–O bond lengths shows that Sr atoms form a highly distorted SrO_8 polyhedron, with a Sr–O mean bond length being 2.699 and 2.676 for Sr_2SmSbO_6 and Sr_2LaSbO_6, respectively; but, in both cases also the distribution of lengths is quite large, ranging from 2.429 to 3.115 in the samarium compound, for instance. The average values of Sr–O bond distances are larger, than the optimal value 2.631 for Sr^{2+} cations in a eight-coordination environment, in both compounds. As mentioned, there is a large size difference between the two *B*-type cations; the Sb^{5+} cation is very much smaller than the Sm^{3+} and the La^{3+} cations: consequently, the distortion is bigger, and, as a result, this gives rise to more enlarged Sr–O bonds. In Fig. 2 we show a clinographic projection of the room-temperature unit cells of Sr_2SmSbO_6, although the angle of rotation of the octahedra is bigger and can be appreciated

Table 1
Crystal structure data and refinement results for Sr_2SmSbO_6 at room temperature.

Atom	Site	x	y	z	B (A^2)
Sm	2*d*	1/2	0	0	0.27(3)
Sb	2*c*	0	1/2	0	0.29(3)
Sr	4*e*	0.0085(8)	0.0333(3)	0.2528(8)	0.61(4)
O1	4*e*	0.286(2)	0.325(2)	0.039(3)	0.88(1)
O2	4*e*	0.308(3)	0.266(3)	0.435(2)	0.88(1)
O3	4*e*	0.904(2)	0.459(3)	0.228(5)	0.88(1)

The atomic positions (in fractional coordinates) and isotropic atomic displacement parameters were refined in the space group $P2_1/n$. (Note: $a = 5.8580(1)$ A; $b = 5.9159(1)$ A; $c = 8.3136(1)$ A; $\beta = 90.23(1)^\circ$; $R_p = 12.0\%$; $R_{wp} = 19.2\%$; $R_{exp} = 15.6\%$; $\chi^2 = 1.50$.)

Table 2
Crystal structure data and refinement results for Sr_2LaSbO_6 at room temperature.

Atom	Site	x	y	z	B (A^2)
La	2*d*	1/2	0	0	0.33(2)
Sb	2*c*	0	1/2	0	0.35(2)
Sr	4*e*	0.0094(4)	0.0344(2)	0.2509(3)	0.85(3)
O1	4*e*	0.269(2)	0.321(2)	0.075(1)	1.08(3)
O2	4*e*	0.312(2)	0.259(2)	0.417(1)	1.08(3)
O3	4*e*	0.879(1)	0.459(1)	0.223(1)	1.08(3)

The atomic positions (in fractional coordinates) and isotropic atomic displacement parameters were refined in the space group $P2_1/n$. (Note: $a = 5.8613(1)$ A; $b = 5.9220(1)$ A; $c = 8.3245(1)$ A; $\beta = 90.25(1)^\circ$; $R_p = 11.8\%$; $R_{wp} = 16.9\%$; $R_{exp} = 10.85\%$; $\chi^2 = 2.41$.)

Table 3
Main bond distances () and selected angles (deg) for Sr_2SmSbO_6 and Sr_2LaSbO_6 from XRPD at room temperature.

	Sr_2SmSbO_6	Sr_2LaSbO_6
Sb–O1 (×2)	1.993(2)	2.000(7)
Sb–O2 (×2)	2.002(7)	2.010(8)
Sb–O3 (×2)	1.998(6)	2.011(2)
Average distance	1.998(5)	2.007(3)
Predicted distance	2.009	2.009
B–O1 (×2)	2.324(2)	2.418(7)
B–O2 (×2)	2.342(7)	2.420(8)
B–O3 (×2)	2.331(6)	2.414(2)
Average distance	2.332(5)	2.417(3)
Predicted distance	2.344	2.428
Sr–O1 (×1)	2.965(2)	2.715(7)
Sr–O1 (×1)	2.429(2)	2.309(7)
Sr–O1 (×1)	2.849(2)	3.167(7)
Sr–O2 (×1)	2.698(7)	2.614(8)
Sr–O2 (×1)	2.471(7)	2.391(8)
Sr–O2 (×1)	3.115(7)	3.239(7)
Sr–O3 (×1)	2.603(7)	2.637(8)
Sr–O3 (×1)	2.466(3)	2.330(5)
Average distance	2.699(6)	2.676(3)
Predicted distance	2.631	2.631
Sb–O1–*B* (×2)	149.1(5)	140.8(3)
Sb–O2–*B* (×2)	146.6(7)	140.0(3)
Sb–O3–*B* (×2)	147.4(2)	140.1(7)
Sb−O−*B*⟩	147.7	140.3

clearly in the figure. Nevertheless, the distortion is bigger, which, as a result, gives rise to a more distorted coordination sphere assigned to Sr^{2+}.

The high distortion, with respect to the prototype structure, observed in both compounds is inferred from the large deviation of the Sb–O–B angle, in both compounds, from the ideal value (180°), as can bee seen in Table 3.

3.2. *High-temperature phase transitions in* Sr_2SmSbO_6 *and* Sr_2LaSbO_6

The thermal evolution of the structures of Sr_2SmSbO_6 and Sr_2LaSbO_6 was studied by means of laboratory X-ray diffraction measurements at different temperatures. In Fig. 3 we show the scattered intensity in the 86−88.5° 2θ interval, projected and represented with shades of gray. Black corresponds to high intensity, and white to low intensity: we have plotted the experimental results for Sr_2SmSbO_6 in panel (a) and for Sr_2LaSbO_6 in panel (b).

As seen in Fig. 3, the distortion of the unit cells gets smaller at higher temperatures: the diffraction lines get closer to each other. At about 885 and 945 K in Sr_2SmSbO_6 and Sr_2LaSbO_6, respectively, as indicated in the figure, the splitting of the diffraction lines reduces appreciably. At those temperatures also, the reflections of the type $h\,k\,l$, with $h+k+l=2n+1$ also disappear in the patterns of both compounds (Fig. 5, panels (b) and (c)). As mentioned, these reflections are characteristic for a primitive unit cell. These observations indicate that, at the mentioned temperatures, the structures transform from the monoclinic symmetry (at low temperature) to another structure of higher symmetry (at high temperature), not with a primitive cell. At about 1170 and 1185 K, in Sr_2SmSbO_6 and in Sr_2LaSbO_6, respectively, the splitting of the diffraction lines disappears, in a continuous way (Fig. 3). This indicates the presence of another phase transition, in each

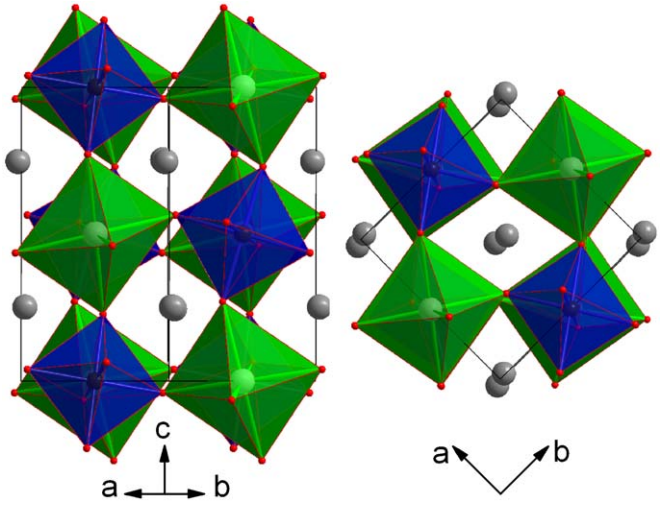

Fig. 2. Clinographic projections of the structures of Sr_2SmSbO_6, along the $[010]_p$ and $[001]_p$ directions, as indicated, in the right and in the left panels, respectively. SmO_6 octahedra are shown green (light), SbO_6 in blue (dark) and Sr cations in gray. (For interpretation of the references to color in this figure legend, the reader is referred to the web version of this article.)

case, that changes the structures from the intermediate to a higher symmetry one, cubic ($Fm\bar{3}m$).

As mentioned in the Introduction, from the structural point of view, different symmetries have been reported for antimony double perovskite materials at room temperature: monoclinic, tetragonal, trigonal and cubic; although, very few temperature-dependent structural studies have been conducted [1,2], so "it is not easy to guess" *a priori*, which could be the expected phase transition sequences. On the other hand, the usual intermediate symmetry between the high- (cubic, $Fm\bar{3}m$) and low-temperature

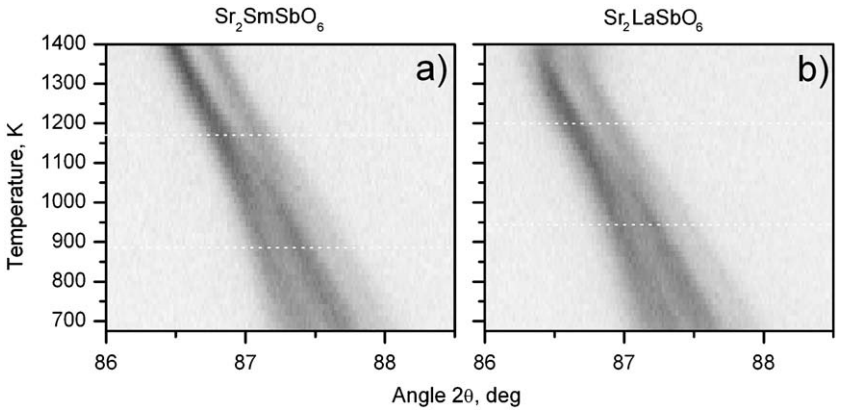

Fig. 3. Thermal evolution of the scattered intensity in the 86–88.5° 2θ interval, projected and represented with shades of gray. Black corresponds to high intensity, and white to low intensity. The horizontal lines are a guide to the eye, and mark the temperatures at which the distortions in both compounds get smaller, first, and, then, disappear; thus, indicating the presence of two successive phase transitions at 885 and 1170 K in Sr_2SmSbO_6; and at 945 and 1185 K in Sr_2LaSbO_6.

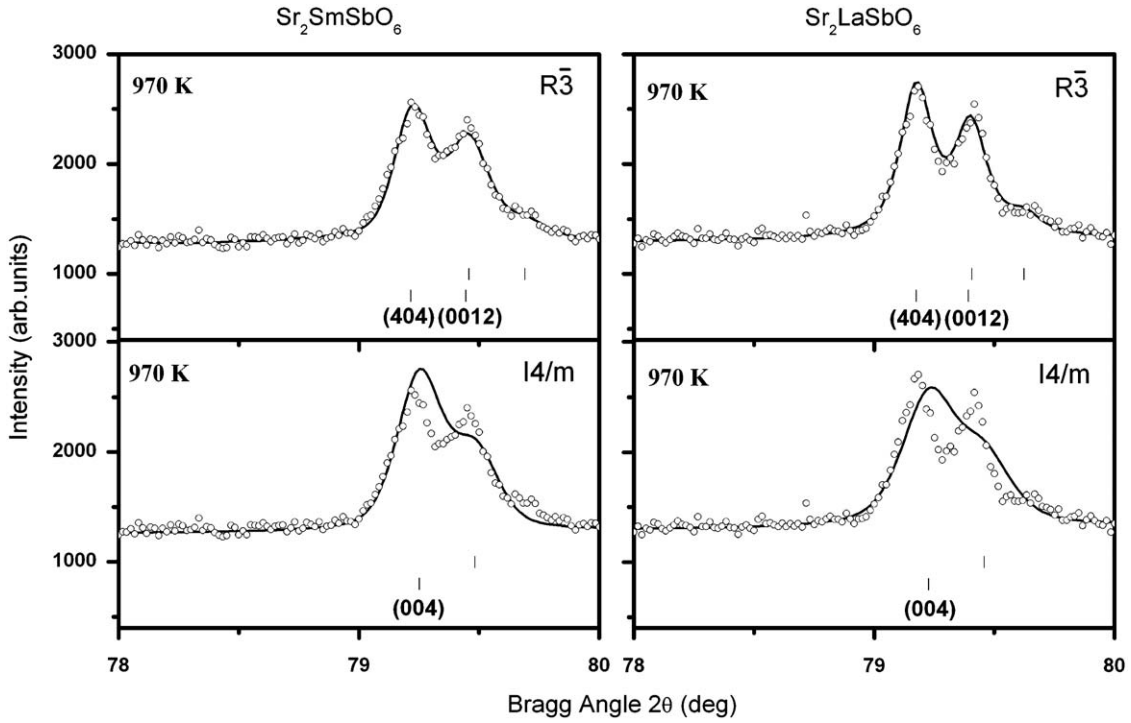

Fig. 4. Results of the refinements, in the 78–80° 2θ interval, in Sr_2SmSbO_6 and Sr_2LaSbO_6, using two different models with the $I4/m$ and $R\bar{3}$ space groups. The bars indicate the Bragg reflections: the lower bars are associated with $K\alpha 1$, and the upper ones with $K\alpha 2$. The tetragonal space group has only one reflection in this 2θ interval, and is unable to take into account of the observed splitting; on the contrary, the trigonal space group has two reflections and takes perfectly into account the splitting.

phases (monoclinic, $P2_1/n$) in the tungstate double perovskites is tetragonal ($I4/m$) [10–12]. So, we attempted to refine the patterns at 970 K, for Sr_2SmSbO_6 and Sr_2LaSbO_6, in the $I4/m$ space group, trying to reproduce the observed splittings, but the results were not satisfactory, as shown in Fig. 4 for Sr_2SmSbO_6 and Sr_2LaSbO_6, respectively. Nevertheless, the structural temperature evolution of the Sr_2CoSbO_6 has been studied and, as reported, shows a first order phase transition from the room-temperature trigonal phase ($R\bar{3}$ space group) to the cubic $Fm\bar{3}m$ space group. The calculated tolerance factors t for both compounds, matched perfectly in Table 1 of [1]. As it can be seen in that table, as the t value increases the stable symmetry at room temperature changes following the next sequence: $P2_1/n \rightarrow I4/m \rightarrow R\bar{3} \rightarrow Fm\bar{3}m$. Increasing temperatures stabilizes more symmetric structures, and as the attempt to refine the structures after the first phase transition using the $I4/m$ space group failed, we tried to refine the patterns of Sr_2SmSbO_6 andSr_2LaSbO_6 after the first transition in the $R\bar{3}$ space group; the results for the same splittings in Fig. 4. These good results confirm that the observed discontinuous phase transition for both compounds is $P2_1/n \rightarrow R\bar{3}$.

The refinement of the structures at 1220 K has confirmed that, at those temperatures, the structures can be described with the $Fm\bar{3}m$ space group (panel (c) Fig. 5). And the patterns collected at temperatures higher than 1185 and 1200 K were well fit by a structural model with the space group $Fm\bar{3}m$, corresponding to the undistorted aristotype double perovskite structure (tilt system $a^0a^0a^0$). No further changes in the set of observed reflections were found above this temperature, suggesting that the type of unit cell does not change up to the highest temperature measured.

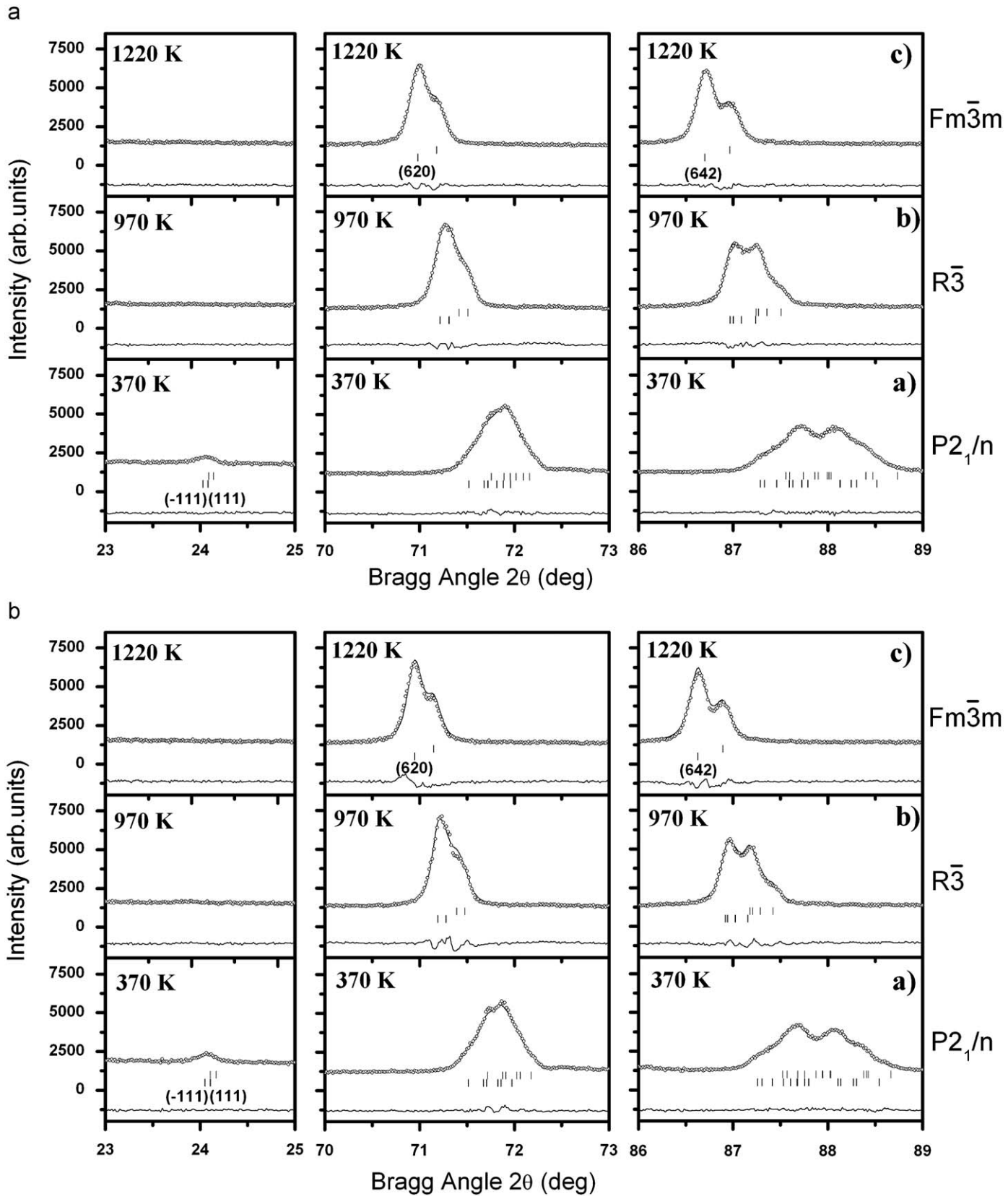

Fig. 5. Temperature evolution of three groups of diffraction peaks located at different 2θ positions. The calculated and the difference diffraction profiles (lines) are obtained after Rietveld refinement of the structure at each temperature. The structural models used in the refinement, for Sr_2SmSbO_6 (upper set) and Sr_2LaSbO_6 (lower set), have the following symmetries: (a) $P2_1/n$ for 370 K, (b) $R\bar{3}$ for 970 K and (c) $Fm\bar{3}m$ for 1120 K. The bars indicate the Bragg reflections: the lower bars are associated with $K\alpha1$, and the upper ones with $K\alpha2$. In the first interval (first column) the monoclinic (−111) and (111) reflections disappear as temperature increases. In the second columns the (620) cubic reflection is shown, which does not split in the trigonal phase. Finally, in the third column, the (642) cubic reflection, clearly splits into two in the trigonal phase.

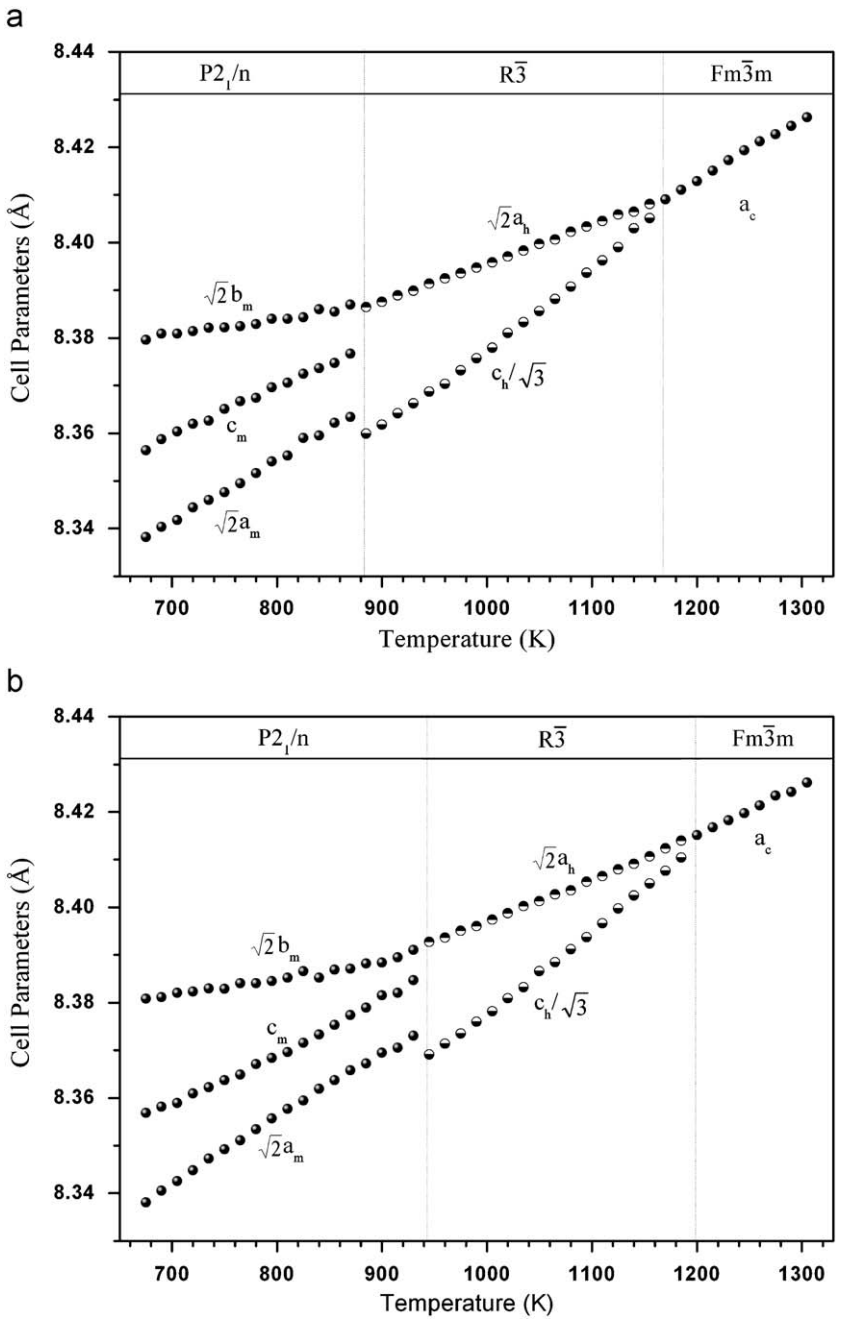

Fig. 6. Temperature evolution of the lattice parameters of (a) Sr_2SmSbO_6 and (b) Sr_2LaSbO_6. We show the cell parameters of the trigonal phase in the hexagonal notation. The monoclinic and hexagonal parameters have been scaled to be comparable with the edge of the centered cubic.

Finally, in Fig. 6 we show the variation with the temperature of the lattice constants of (a) Sr_2SmSbO_6 and (b) Sr_2LaSbO_6. The monoclinic and hexagonal parameters have been scaled to be comparable with the edge of the centered cubic as it appears in the final structure. In both compounds Sr_2SmSbO_6 and Sr_2LaSbO_6, the transitions are clearly seen. At about 885 and 945 K in Sr_2SmSbO_6 and Sr_2LaSbO_6, respectively, we can see a discontinuous variation of parameters indicative of the first order nature of the corresponding transition from monoclinic symmetry $P2_1/n$ to trigonal symmetry $R\bar{3}$. And about 1170 K for samarium compound and about 1185 K for the lanthanum compound, a continuous variation of parameters is observed, indicative of the second order nature of the corresponding transition from $R\bar{3}$ to $Fm\bar{3}m$.

Thus, the structural analysis of Sr_2SmSbO_6 and Sr_2LaSbO_6 suggests that there is a two phase transitions at high temperatures, the first one being discontinuous and the second one continuous as a following phase transition sequence: $P2_1/n \rightarrow R\bar{3} \rightarrow Fm\bar{3}m$. As far as we know, this is the first time that a double phase transition sequence, from primitive monoclinic $P2_1/n$ at room temperature to cubic symmetry $Fm\bar{3}m$ at high temperature with a trigonal intermediate phase, is observed in the antimony double perovskites. The $R\bar{3}$ space group as a high-temperature intermediate symmetry was previously reported for Ba_2PrNbO_6, but with a centred monoclinic symmetry ($I2/m$) at room temperature [13,14]. Phase transition sequences with two phase transitions have been observed also for Sr_2CrSbO_6 with a different phase transition sequence: $I2/m \rightarrow I4/m \rightarrow Fm\bar{3}m$ [2], for

instance, in which the intermediate phase is tetragonal. The mechanism of these discontinuous phase transitions is related to the mismatch of the size of the *A* cation and the cuboctahedral space between the BO_6 and SbO_6 octahedra. The big difference between the *B* cations' radii could be responsible for bringing the intermediate phase to a trigonal structure, more symmetric than the tetragonal structure.

4. Conclusions

The new double perovskites Sr_2SmSbO_6 and Sr_2LaSbO_6 have structures with $P2_1/n$ space group symmetry at room temperature, resulting from Sm(La)/Sb ordering and $(a^+b^-b^-)$ tilt system. The temperature evolution of the structures of Sr_2SmSbO_6 and Sr_2LaSbO_6 show the following sequence of two phase transitions: $P2_1/n \rightarrow R\bar{3} \rightarrow Fm\bar{3}m$, a discontinuous one, at 885 and 945 K, for Sr_2SmSbO_6 and Sr_2LaSbO_6, respectively; and a continuous one, at 1170 and 1185 K, for Sr_2SmSbO_6 and Sr_2LaSbO_6, respectively. This sequence $P2_1/n \rightarrow R\bar{3} \rightarrow Fm\bar{3}m$ of structural transitions has been observed for the first time in the antimony double perovskite family.

Acknowledgments

This work was done in part under project numbers: UPV 0063.310-13564/2001-2007 and MAT2008-05839/MAT. Two of the authors, E. Iturbe-Zabalo and I. Urcelay-Olabarria, thank the grants received from the ILL (MBR-GL/09-056) and from the University of the Basque Country UPV/EHU (Grant PIFA01/2008/044), respectively, to carry part of the present work.

References

[1] A. Faik, M. Gateshki, J.M. Igartua, J.L. Pizarro, M. Insausti, R. Kaindl, A. Grzechnik, J. Solid State Chem. 181 (2008) 1759–1766.
[2] A. Faik, J.M. Igartua, M. Gateshki, G.J. Cuello, J. Solid State Chem. 2009, YJSSC12905.
[3] J. Rodríguez-Carvajal, Physica B 192 (1993) 55–69.
[4] A.M. Glazer, Acta Crystallogr. B 28 (1972) 3384–3392;
A.M. Glazer, Acta Crystallogr. A 31 (1975) 756–762.
[5] C.J. Howard, B.J. Kennedy, P.M. Woodward, Acta Crystallogr. B 59 (2003) 463–471.
[6] E.J. Cussen, J.F. Vente, P.D. Battle, T.C. Gibb, J. Mater. Chem. 7 (1997) 459–463.
[7] H. Karunadasa, Q. Huang, B.G. Ueland, P. Schiffer, R.J. Cava, PNAS V100 (2003) 8097–8102.
[8] R.D. Shannon, Acta Crystallogr. A 32 (1976) 751.
[9] I.D. Brown, D. Altermatt, Acta Crystallogr. B 41 (1985) 244–247.
[10] M. Gateshki, J.M. Igartua, E. Hernández-Bocanegra, J. Phys. Cond. Matter 15 (2003) 6199–6217.
[11] M. Gateshki, J.M. Igartua, J. Phys. Cond. Matter 16 (2004) 6639–6649.
[12] M. Gateshki, J.M. Igartua, A. Faik, J. Solid State Chem. 180 (2007) 2248–2255.
[13] R.H. Mitchell, Perovskites. Modern and Ancient, Almaz Press, 2002.
[14] P.J. Saines, J.R. Spencer, B.J. Kennedy, Y. Kubota, C. Minakata, H. Hano, K. Kato, M. Takata, J. Solid State Chem. 180 (2007) 3001–3007.